JOURNAL OF GUIDANCE, CONTROL, AND DYNAMICS
Vol. 28, No. 1, January–February 2005

# Flight Control Design of an Unmanned Space Vehicle Using Gain Scheduling

Atsushi Fujimori*
*Shizuoka University, Hamamatsu 432-8561, Japan*
Fuyuto Terui†
*National Aerospace Laboratory, Tokyo 182-8522, Japan*
and
Peter N. Nikiforuk‡
*University of Saskatchewan, Saskatoon, Saskatchewan S7N 5A9, Canada*

**A flight control design of an unmanned space vehicle using an interpolative gain-scheduling technique is presented. The $\nu$-gap metric is used to evaluate the interpolative errors between linear models at operating points. The linear-parameter-varying models for the space vehicle are then constructed by minimizing a criterion using the $\nu$-gap metric. Furthermore, multi-objective constraints are locally imposed on the specified operating points to improve the control performance. In the numerical simulations, the gain-scheduling control laws whose number of operating points was greater than two stabilized the space vehicle over the entire region. Furthermore, the input-saturation constraint was effective in suppressing the magnitude of the input and extending the stability region of the design parameter.**

## I. Introduction

THE National Aerospace Laboratory and the National Aerospace Development Agency in Japan had been developing an unmanned reentry space vehicle, named HOPE-X, for a decade.[1–9] It had been planned that the vehicle would be used to transport materials between the Earth and the International Space Station. Unfortunately, this project has been suspended. Nevertheless, it is still worthwhile to study fundamental techniques for developing future reusable space vehicles. The mission profile of the HOPE-X was planned as follows.[3] The HOPE-X vehicle would be launched by a Japanese rocket, H-IIA, from Tamegashima in Japan. At the height of about 110 km, the HOPE-X vehicle would separate from the H-IIA and enter into a low Earth orbit. After one revolution around the Earth, the vehicle would deorbit and reenter the atmosphere. The flight path and the attitude are controlled by reaction control systems and aerodynamic surfaces. There are three flight profiles after the deorbit: reentry phase, terminal area energy management (TAEM) phase,[10] and automatic landing phase. In Ref. 9, a flight control system of the HOPE-X vehicle in the TAEM phase was designed by a linear-interpolative gain-scheduling technique. A plant model of the HOPE-X vehicle was first expressed as a linear-parameter-varying (LPV) model. To guarantee global stability over the entire operating region, a quadratic stability constraint with using the Lyapunov function was imposed. The constraint was transformed into linear matrix inequalities (LMIs).[11] A control law was then calculated to satisfy the LMIs. In Ref. 9, two types of control laws were proposed, and their effectiveness was demonstrated by numerical simulation using Simulink.[4] However, it was not clear how the operating points for constructing the LPV model should be selected. In addition, the HOPE-X vehicle sometimes destabilized for a large guidance command.[9] Therefore, the gain-scheduling control law needs to be improved to avoid such destabilization.

To overcome these points, this paper proposes a method for selecting the operating points in which the $\nu$-gap metric[12] is used to evaluate the interpolative error between the operating points. Furthermore, multi-objective constraints are locally imposed on the specified operating points to improve the control performance. The effectiveness of the proposed technique is evaluated by the numerical simulation of the HOPE-X.

## II. LPV System of HOPE-X Vehicle

The equation of motion of the HOPE-X vehicle is written as a nonlinear equation:

$$\begin{aligned} \dot{x}(t) &= f(x(t), u(t)) \\ z(t) &= g(x(t), u(t)) \end{aligned} \tag{1}$$

where $u(t)$, $z(t)$, and $x(t)$ are $m$-dimensional input, $p$-dimensional controlled variable, and $n$-dimensional state vectors, respectively. It is assumed that $x(t)$ is available for feedback. Because a reference trajectory for the HOPE-X vehicle is given in advance,[10] it is sufficient to take into consideration the dynamics governed by Eq. (1) near the reference trajectory. Letting $\theta(t)$ be a varying parameter identifying the reference trajectory, $r$ operating points, that is, the linearized points, are selected on the reference trajectory

$$\theta_1 < \cdots < \theta_r \tag{2}$$

Denoting the linearized point as $(x_i^d, u_i^d)$ at each point $\theta_i$, the linear-time-invariant (LTI) model is given by

$$\begin{bmatrix} \dot{x}(t) \\ z(t) \end{bmatrix} = \begin{bmatrix} A_i & B_i \\ C_i & D_i \end{bmatrix} \begin{bmatrix} x(t) - x_i^d \\ u(t) - u_i^d \end{bmatrix} + \begin{bmatrix} 0 \\ z_i^d \end{bmatrix}$$

$$\text{for} \qquad \theta = \theta_i \quad (i = 1, \ldots, r) \tag{3}$$

where

$$A_i \triangleq \frac{\partial f\left(x_i^d, u_i^d\right)}{\partial x^T}, \qquad B_i \triangleq \frac{\partial f\left(x_i^d, u_i^d\right)}{\partial u^T}$$

Presented as Paper 2003-5414 at the AIAA Guidance, Navigation, and Control Conference, Austin, TX, 11–14 August 2003; received 11 September 2003; revision received 19 February 2004; accepted for publication 19 February 2004. 

*Associate Professor, Department of Mechanical Engineering, 3-5-1 Johoku; tmafuji@ipc.shizuoka.ac.jp. Member AIAA.
†Researcher, Space Technology Research Group, 7-44-1 Shindaiji-Higashi, Chofu. Member AIAA.
‡Dean Emeritus, Department of Mechanical Engineering.

$$C_i \triangleq \frac{\partial g\left(x_i^d, u_i^d\right)}{\partial x^T}, \qquad D_i \triangleq \frac{\partial g\left(x_i^d, u_i^d\right)}{\partial u^T}$$

Using the linear-interpolation between the LTI models, the LPV model approximating Eq. (1) over the specified trajectory ($\theta_1 \le \theta \le \theta_r$) is then expressed as

$$\begin{bmatrix} \dot{x}(t) \\ z(t) \end{bmatrix} = \begin{bmatrix} A(\theta) & B(\theta) \\ C(\theta) & D(\theta) \end{bmatrix} \begin{bmatrix} x(t) - x^d(\theta) \\ u(t) - u^d(\theta) \end{bmatrix} + \begin{bmatrix} 0 \\ z^d(\theta) \end{bmatrix} \quad \text{for} \quad \theta \in [\theta_i, \theta_{i+1}] \tag{4}$$

where

$$\begin{bmatrix} A(\theta) & B(\theta) \\ C(\theta) & D(\theta) \end{bmatrix} = \mu_i(\theta) \begin{bmatrix} A_i & B_i \\ C_i & D_i \end{bmatrix} + \mu_{i+1}(\theta) \begin{bmatrix} A_{i+1} & B_{i+1} \\ C_{i+1} & D_{i+1} \end{bmatrix} \tag{5}$$

$$\begin{bmatrix} x^d(\theta) \\ u^d(\theta) \end{bmatrix} = \mu_i(\theta) \begin{bmatrix} x_i^d \\ u_i^d \end{bmatrix} + \mu_{i+1}(\theta) \begin{bmatrix} x_{i+1}^d \\ u_{i+1}^d \end{bmatrix} \tag{6}$$

$$\mu_i(\theta) \triangleq \frac{\theta_{i+1} - \theta}{\theta_{i+1} - \theta_i}, \qquad \mu_{i+1}(\theta) \triangleq \frac{\theta - \theta_i}{\theta_{i+1} - \theta_i} \tag{7}$$

That is, matrices $A(\theta)$, $B(\theta)$, $C(\theta)$, and $D(\theta)$ are given so as to linearly interpolate the intermediate region between neighboring operating points.

## III. Operating Point Selection Using $\nu$-Gap Metric

The LPV model of the nonlinear equation was constructed as described in the preceding section. However, the quality of the LPV model, that is, whether the LPV model Eq. (4) properly approximates the original nonlinear system Eq. (1) or not, depends on the operating points. In this paper, the $\nu$-gap metric[12] is used as a criterion for selecting the operating points, that is, to evaluate the interpolative error of Eq. (4). The $\nu$-gap metric was originally introduced to discuss the robust stability related to the stability margin. This section briefly explains the $\nu$-gap metric and the stability margin. A method for selecting the operating points with the $\nu$-gap metric is then proposed.

### A. Robust Stability and $\nu$-Gap Metric

Let $P(s)$ be a plant model of a $m$-input and $p$-output controlled system. Denoting a class of stabilizing controllers for $P(s)$ as $\Omega(P)$, the stability margin of a controller $K(s) \in \Omega(P)$ is defined as follows[12]:

$$b_{P,K} \triangleq \inf_{\omega} \rho(P(j\omega), K(j\omega)) \tag{8}$$

where

$$\rho(X, Z) \triangleq 1/\bar{\sigma}\left(\begin{bmatrix} X \\ I \end{bmatrix} (I - ZX)^{-1} [-Z \quad I]\right)$$

where $\bar{\sigma}(\cdot)$ means the maximum singular value. The range of $b_{P,K}$ is given by $b_{P,K} \in [0, \quad 1]$. $b_{P,K}$ is originally derived from the Nyquist criterion for multivariable systems in terms of normalized left coprime fractional representation.[12,13]

On the other hand, let $P_1(s)$ and $P_2(s)$ be two plant models for a controlled system. Then, the difference between $P_1(s)$ and $P_2(s)$, that is, the $\nu$-gap metric, is defined as follows[12]:

$$\delta_\nu(P_1, P_2) \triangleq \sup_{\omega} \kappa(P_1(j\omega), P_2(j\omega)) \tag{9}$$

where

$$\kappa(X, Y) \triangleq \bar{\sigma}\left((I + YY^*)^{\frac{1}{2}}(Y - X)(I + XX^*)^{\frac{1}{2}}\right)$$

The range of $\delta_\nu(P_1, P_2)$ is also given by $\delta_\nu(P_1, P_2) \in [0, \quad 1]$. If the controlled system has a single input and a single output, Eq. (9) can be written as

$$\delta_\nu = \sup_{\omega} \frac{|P_2(j\omega) - P_1(j\omega)|}{\sqrt{1 + |P_1(j\omega)|^2}\sqrt{1 + |P_2(j\omega)|^2}} \tag{10}$$

Equation (10) means the distance between $P_1(j\omega)$ and $P_2(j\omega)$ on the Riemann sphere.

Using the stability margin and the $\nu$-gap metric, the robust stability is summarized by the following theorem[12]:

*Theorem 1:* Supposing $K \in \Omega(P_1)$, the following relations hold:

$$(1)\ K \in \{\Omega(P_2), \delta_\nu(P_1, P_2) \le \beta\} \Leftrightarrow b_{P_1,K} > \beta \tag{11}$$

$$(2)\ \left\{K, b_{P_1,K} > \beta\right\} \in \Omega(P_2) \Leftrightarrow \delta_\nu(P_1, P_2) \le \beta \tag{12}$$

□

Theorem 1 indicates that a controller $K$ whose $b_{P_1,K}$ is large can stabilize $P_2$ whose $\delta_\nu(P_1, P_2)$ is large. Alternatively, a plant model $P_2$ whose $\delta_\nu(P_1, P_2)$ is small can reduce the lower bound of the stability margin to guarantee the robust stability. From the quantitative point of view, a sufficient condition for the robust stability is $b_{P_1,K} > \delta_\nu(P_1, P_2)$, where $P_1(s)$ and $P_2(s)$ are respectively regarded as a designed (nominal) model and a perturbed model. This paper uses the latter concept, that is, the operating points for constructing the LPV model are selected so as to optimize a criterion using the $\nu$-gap metric.

### B. Criteria with $\nu$-Gap Metric

This paper proposes two types of the criteria using the $\nu$-gap metric to select the operating points of the LPV model. Let $P_{\mathrm{lpv}}(s; \theta)$ and $P(s; \theta)$ be transfer functions of the LPV and the LTI model at the operating point $\theta$, respectively. Then, the following criteria are proposed to evaluate the interpolative error of the LPV model over the entire operating region:

$$I_p \triangleq \max_{\theta_1 \le \theta \le \theta_r} \delta_\nu(P_{\mathrm{lpv}}(j\omega; \theta), P(j\omega; \theta)) \tag{13}$$

$$I_a \triangleq \int_{\theta_1}^{\theta_r} \delta_\nu(P_{\mathrm{lpv}}(j\omega; \theta), P(j\omega; \theta))\, \mathrm{d}\theta \tag{14}$$

where $I_p$ is the maximum of the $\nu$-gap metric over the entire operating region and $I_a$ is the error area. That is, the operating points of the LPV model are selected so as to minimize either $I_p$ or $I_a$.

## IV. Local Multi-Objective Gain Scheduling

In general, it is not necessarily required that the control constraints—the stability, tracking, disturbance rejection, etc.—are uniformly imposed over the entire operating region. In an operating region where a large tracking command is made, an additional constraint should be imposed to improve the tracking. On the other hand, in an operating region where the parameters of the plant are violently changed the stability margin of the closed-loop system should be increased. Therefore, the control constraints should be imposed according to the control requirements of the operating region. Then, this paper uses local multi-objective gain scheduling in which additional constraints are locally imposed on the specified operating points. The additional constraint used in this paper is a constraint for suppressing the magnitude of input, that is, the input-saturation constraint is considered.

The gain-scheduling state feedback law for Eq. (4) is written as

$$u(t) = -F(\theta)x(t) \qquad F \in \Re^{m \times n} \tag{15}$$

If the closed-loop matrix $A(\theta) - B(\theta)F(\theta)$ is a stable matrix over the entire operating region, the closed-loop system is globally stable. To guarantee the global stability, consider the following parameter-dependent Lyapunov function[14]:

$$V(t) = x^T(t)P(\theta)x(t) \qquad P(\theta) \in \Re^{n \times n} > 0 \tag{16}$$

where $P(\theta)$ is a positive matrix with the varying parameter $\theta$. Then, $\mathrm{d}V/\mathrm{d}t$ is given by

$$\frac{\mathrm{d}V}{\mathrm{d}t} = \dot{x}^T P x + x^T P \dot{x} + x^T \frac{\mathrm{d}P}{\mathrm{d}t} x \tag{17}$$

Differentiating $PP^{-1} = I$ by $t$ gives

$$\frac{\mathrm{d}P}{\mathrm{d}t} P^{-1} + P \frac{\mathrm{d}P^{-1}}{\mathrm{d}t} = 0$$

Then,

$$\frac{\mathrm{d}P}{\mathrm{d}t} = -P \frac{\mathrm{d}P^{-1}}{\mathrm{d}t} P = -P\dot{\theta} \frac{\mathrm{d}P^{-1}}{\mathrm{d}\theta} P \tag{18}$$

A sufficient condition of the quadratic stability is given by[6,7]

$$\dot{V}(t) < -x^T (Q + F^T R F) x \tag{19}$$

where $Q \in \Re^{n\times n} \geq 0$, $R \in \Re^{m\times m} > 0$ are weighting matrices and remained to be designed. Letting $X(\theta) \stackrel{\Delta}{=} P^{-1}(\theta)$ and $F(\theta)X(\theta) \stackrel{\Delta}{=} M(\theta) \in \Re^{m\times n}$, inequality (19) is transformed into the following matrix inequality:

$$AX + XA^T - BM - M^T B^T - \dot{\theta} \frac{\mathrm{d}X}{\mathrm{d}\theta} + XQX + M^T R M < 0 \tag{20}$$

To express matrix inequality (20) finitely, $M(\theta)$ and $X(\theta)$ are linearly interpolated as

$$M(\theta) = \mu_i(\theta) M_i + \mu_{i+1}(\theta) M_{i+1} \tag{21}$$

$$X(\theta) = \mu_i(\theta) X_i + \mu_{i+1}(\theta) X_{i+1} \tag{22}$$

Using Eq. (22), $\mathrm{d}X/\mathrm{d}\theta$ is obtained as

$$\frac{\mathrm{d}X}{\mathrm{d}\theta} \simeq \frac{X_{i+1} - X_i}{\theta_{i+1} - \theta_i} \stackrel{\Delta}{=} \left( \frac{\Delta X}{\Delta \theta} \right)_i \tag{23}$$

Substituting Eqs. (21–23) into Eq. (20) and using the Schur complement,[11] LMIs with respect to $X_i$ and $M_i$ $(i = 1, \ldots, r)$ are derived as follows:

$$X_i > 0 \qquad (i = 1, \ldots, r) \tag{24a}$$

$$\begin{bmatrix} A_i X_i + X_i A_i^T - B_i M_i & \star & \star \\ -M_i^T B_i^T - \omega(\Delta X/\Delta\theta)_i & & \\ H X_i & -I_q & \star \\ M_i & 0 & -R^{-1} \end{bmatrix} < 0 \tag{24b}$$

$$\begin{bmatrix} A_j X_j + X_j A_j^T - B_j M_j & \star & \star \\ -M_j^T B_j^T - \omega(\Delta X/\Delta\theta)_i & & \\ H X_j & -I_q & \star \\ M_j & 0 & -R^{-1} \end{bmatrix} < 0 \tag{24c}$$

$$\begin{bmatrix} A_i X_j + A_j X_i + X_j A_i^T & & \\ +X_i A_j^T - B_i M_j & & \\ -B_j M_i - M_j^T B_i^T & \star & \star \\ -M_i^T B_j^T - 2\omega(\Delta X/\Delta\theta)_i & & \\ H(X_i + X_j) & -2I_q & \star \\ M_i + M_j & 0 & -2R^{-1} \end{bmatrix} < 0 \tag{24d}$$

$$\omega \stackrel{\Delta}{=} \dot{\theta}_{\max}, \qquad \dot{\theta}_{\min} \qquad (i = 1, \ldots, r-1,\ j = i+1) \tag{24e}$$

where $\mathrm{rank}\, Q = q$ and $Q = H^T H$, $H \in \Re^{q\times n}$, $\star$ means the transpose of the elements located at diagonal position, and $\dot{\theta}_{\max}$ and $\dot{\theta}_{\min}$ are respectively the maximum and the minimum of $\dot{\theta}$, that is, LMIs (24b), (24c), and (24d) are doubled with respect to $\omega$. The number of LMIs to be satisfied is $r + (r-1) \times 3 \times 2 = 7r - 6$.

As will be shown in the numerical simulation of the HOPE-X, a large roll angle command is required at the beginning of the TAEM phase. In a previous study,[9] the HOPE-X vehicle was sometimes destabilized by saturating control surface angles large roll-angle commands. To avoid this saturation, an additional constraint is locally imposed on the specified operating points. It is given by

$$V(x(0)) < \rho^2 \qquad \rho > 0 \tag{25}$$

The purpose of this constraint is to suppress the time response for the initial state. As a matter of fact, a constraint $\|u(t)\| < \rho$ should be imposed to suppress the saturation of the control input. In the time response of the initial state, $V[x(t)] \leq V[x(0)]$ holds $\forall t > 0$ if the closed-loop system is stable. If constraint (25) and the following relations are satisfied,

$$u^T(t) u(t) < V(x(t)) \tag{26}$$

and

$$u^T(t) u(t) = x^T(t) F^T F x(t) < x^T(t) P x(t) \leq x^T(0) P x(0) < \rho^2$$

inequalities (25) and (26) are sufficient constraints for $\|u(t)\| < \rho$. Using $X$ and $M$ instead of $P$ and $F$, inequalities (25) and (26) are transformed into

$$\rho^2 - x^T(0) X^{-1} x(0) > 0 \tag{27a}$$

$$X - M^T M > 0 \tag{27b}$$

where inequality (27a) is a constraint for making $X$ large and inequality (27b) is a constraint for making $M$ small. As a result, the obtained state feedback gain $F = MX^{-1}$ might be too small. It is for this reason that in this paper only inequality (27a) is employed, that is, Eq. (25) is used as an additional local constraint to improve the control performance and avoid conservative state feedback gain.

Let $r_a$ be the number of the operating points imposing the local constraint (25) and $C_a$ be the class of the imposed operating points. The following additional LMIs are then imposed and must be satisfied:

$$\begin{bmatrix} X_i & x(0) \\ x^T(0) & \rho^2 \end{bmatrix} > 0 \qquad \text{for} \qquad \theta_i \in C_a (i = 1, \ldots, r_a) \tag{28}$$

Thus, if $X_i$ and $M_i$ satisfying LMIs (24) and (28) are found the feedback gain $F(\theta)$ is given by

$$F(\theta) = [\mu_i(\theta) M_i + \mu_{i+1}(\theta) M_{i+1}][\mu_i(\theta) X_i + \mu_{i+1}(\theta) X_{i+1}]^{-1}$$
$$\text{for} \qquad \theta \in [\theta_i, \theta_{i+1}] \tag{29}$$

## V. Numerical Simulation in TAEM Phase

The proposed operating point selection method and the local multi-objective gain-scheduling technique were evaluated in the numerical simulation of the HOPE-X. The flight profile of the HOPE-X after deorbit consisted of the following three parts: reentry phase, TAEM phase, and automatic landing phase. In this paper, the flight control system for the TAEM phase was considered. In the TAEM phase, the range of the altitude $H$ and the Mach number $M$ were given as $3 \leq H \leq 28$ km and $0.5 \leq M \leq 2.5$, respectively. Figure 1 shows the flight control system, which was constructed in Simulink.[4] The nonlinear equation (1) was embedded in the block of "Dynamics of HOPE-X vehicle." The sensor-measured variables were fed into the guidance law to generate the guidance commands. They were fed into the control law to calculate the control surface angles for stabilizing the vehicle. Both the guidance and the control laws respectively divided into the longitudinal and lateral directions. The gain-scheduling proposed in this paper was then separately applied to the design of the control law in the longitudinal and lateral directions.

In Eqs. (1) and (4), the state variable $x$, the input $u$, and the controlled variable $z$ of the longitudinal and the lateral directions were respectively given as follows:

Longitudinal model:

$$x = [\alpha \quad q]^T, \qquad u = \delta_e, \qquad z = a_z$$

Lateral model:

$$x = [\beta \quad p \quad r \quad \phi]^T, \qquad u = [\delta_a \quad \delta_r]^T, \qquad z = [\phi \quad a_y]^T$$

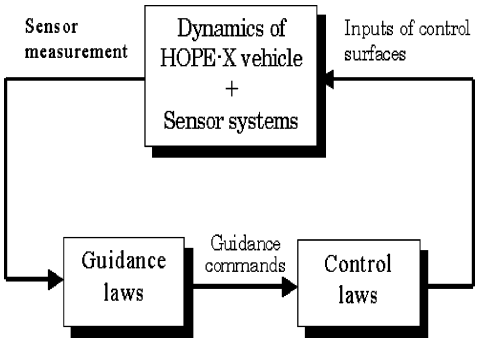


**Fig. 1 Flight control system of HOPE-X vehicle.**

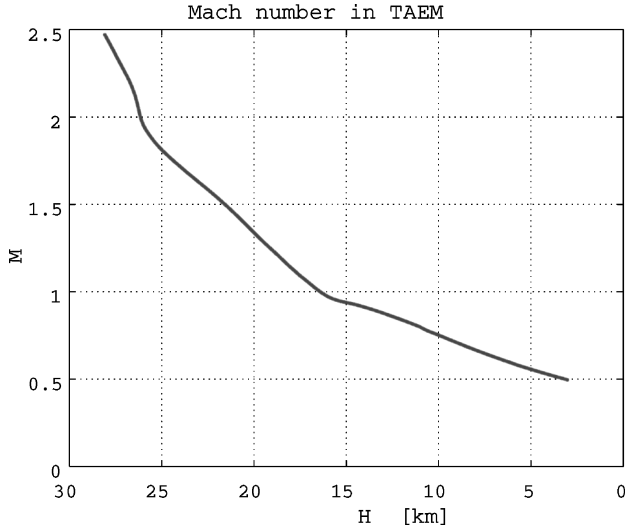


**Fig. 2 Mach number $M$ with respect to the altitude $H$ in TAEM phase.**

where $\alpha$ is the angle of attack, $q$ the pitch angular velocity, $\beta$ the sideslip angle, $p$ the roll angular velocity, $r$ the yaw angular velocity, and $\phi$ the roll angle. They were assumed to be measurable. $\delta_e$ was the elevator angle, $\delta_a$ the aileron angle, and $\delta_r$ the rudder angle, and $a_z$ and $a_y$ were respectively the vertical and the lateral acceleration.

In the TAEM phase, the altitude $H$ was proportionally decreased with respect to the time $t$ and the Mach number $M$ was also monotonously decreased with respect to $H$ as shown in Fig. 2. In this paper, therefore, $M$ was used as the varying parameter $\theta(t)$ for constructing the LPV model.

### A. $\nu$-Gap Metric and LPV Model in TAEM Phase

To check the model error in the TAEM phase, the $\nu$-gap metric $\delta_\nu[P(j\omega; M), P(j\omega; M_0)]$ between the LTI models in which the nominal point, denoted as $M_0$, was selected as $M_0 = 0.5$, 1.5, and 2.5 is shown by the solid line in Figs. 3, 4, and 5, respectively. $\delta_\nu$ increased when the Mach number was shifted from the nominal point. The stability margin $b_{P,K}$ of a fixed-state feedback law, which was designed at each nominal point, is shown by the dashed line in Figs. 3–5. From Theorem 1, the closed-loop system is robustly stable only if $b_{P,K} > \delta_\nu$, where $b_{P,K}$ in the longitudinal direction was larger than that in the lateral direction at each nominal point. This meant that the longitudinal motion of the HOPE-X vehicle might be stabilized by a fixed control law, but the lateral motion might not be. That is, it was indicated that gain scheduling was needed for the lateral direction.

In the lateral direction, $b_{P,K}$ whose nominal point was $M_0 = 2.5$ (Fig. 5b) was smaller than the one whose nominal point was $M_0 = 0.5$ (Fig. 3b) and 1.5 (Fig. 4b), but the stabilized operating region was wider. This meant that the robust stability condition $b_{P,K} > \delta_\nu$ was sufficient for a specified perturbation and the stability region was not uniform to all parameter changes.

Figures 6–9 show the stability margin $b_{P_{\text{lpv}},K}$ and the $\nu$-gap metric $\delta_\nu[P_{\text{lpv}}(j\omega; M), P(j\omega; M)]$ between the LPV and the LTI models in which the number of the operating points was $r = 2 \sim 5$ and they were obtained so as to minimize $I_p$. The Mach number with $\delta_\nu = 0$ means the selected operating point. It is seen that the peak of $\delta_\nu$ was reduced by increasing the number of the operating points $r$. Especially at $r = 5$ in the longitudinal direction (Fig. 9a), $\delta_\nu$ was smaller than $b_{P_{\text{lpv}},K}$ over the entire operating region, that is, the robust stability was guaranteed.

### B. Simulation Results with Respect to Number of Operating Points

Using the operating points obtained by minimizing $I_p$ or $I_a$, LPV models were constructed and gain-scheduling state feedback laws were designed for the number of the operating points $r = 2 \sim 5$. They were embedded in the Simulink simulation of the HOPE-X.

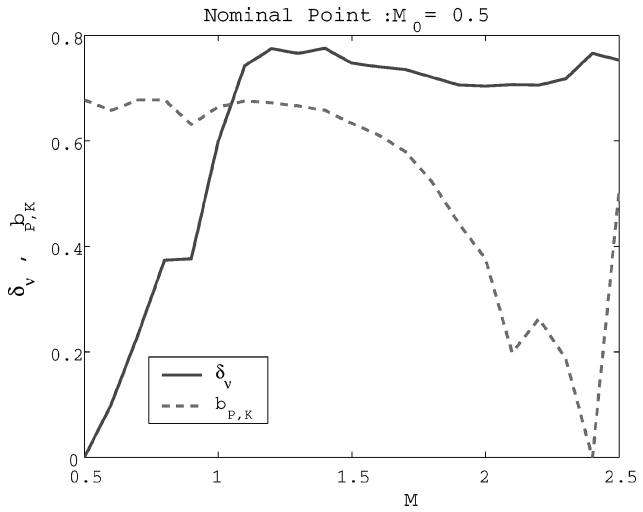


a)

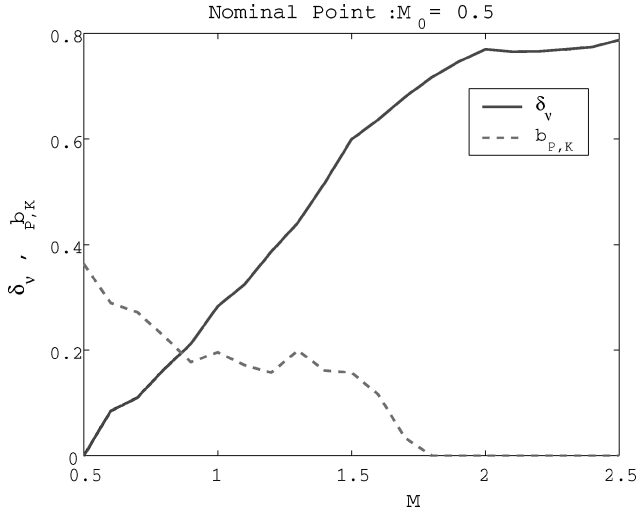


b)

**Fig. 3 $\nu$-gap metric $\delta_\nu[P(j\omega; M), P(j\omega; M_0)]$ between LTI models and stability margin $b_{P,K}$ of closed loop with fixed-state feedback designed at nominal point $M_0 = 0.5$: a) longitudinal and b) lateral direction.**

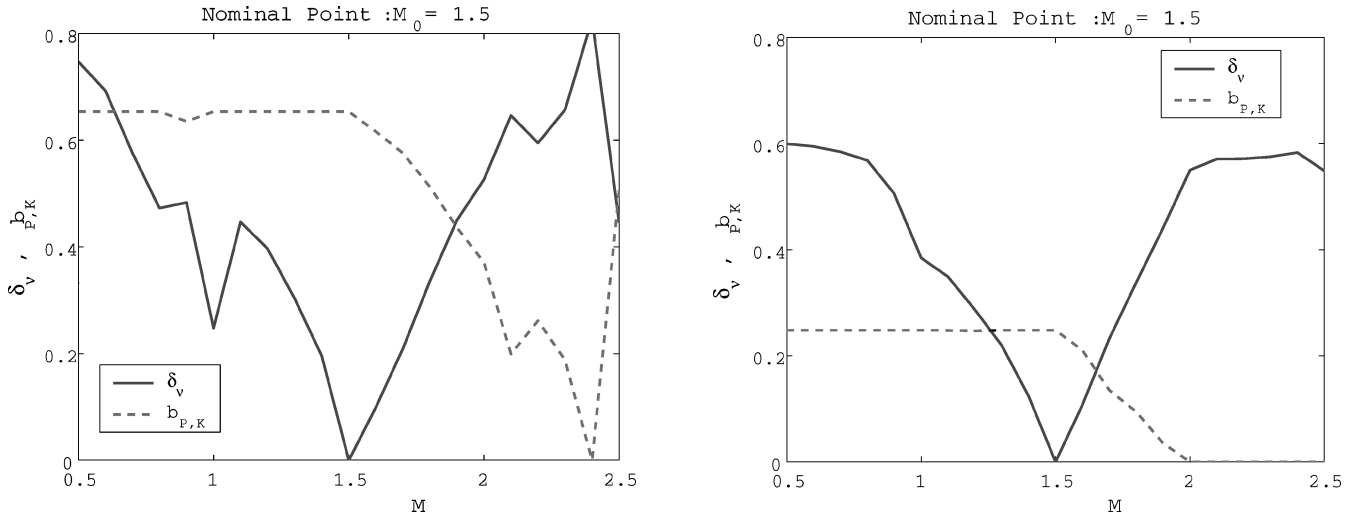


a) b)

**Fig. 4** $\nu$-gap metric $\delta_\nu[P(j\omega; M), P(j\omega; M_0)]$ between LTI models and stability margin $b_{P,K}$ of closed loop with fixed-state feedback designed at nominal point $M_0 = 1.5$: a) longitudinal and b) lateral direction.

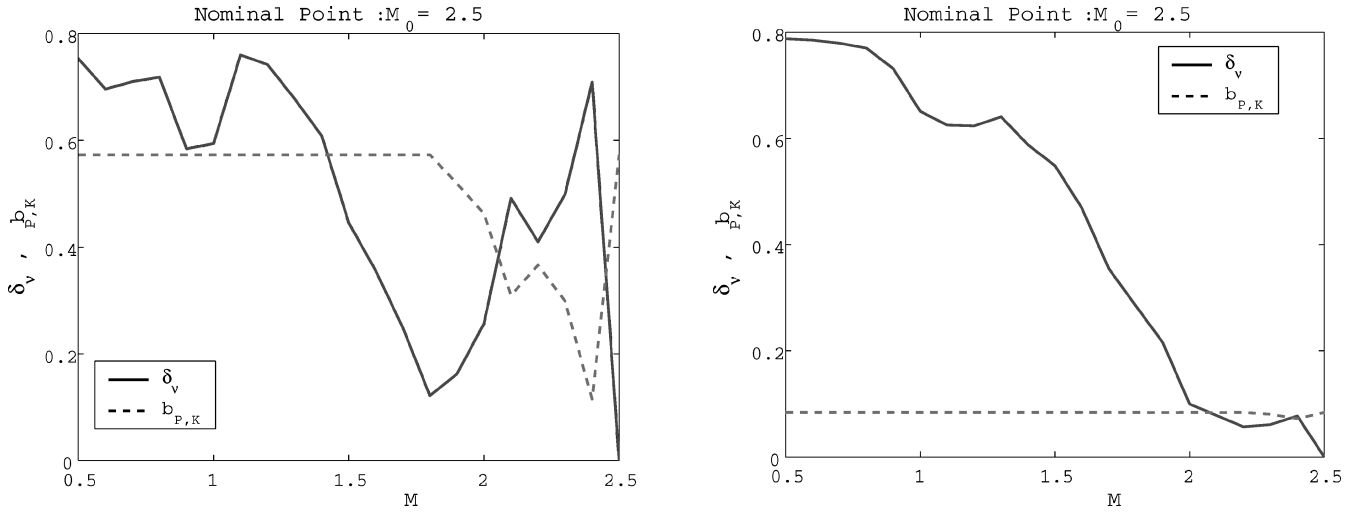


a) b)

**Fig. 5** $\nu$-gap metric $\delta_\nu[P(j\omega; M), P(j\omega; M_0)]$ between LTI models and stability margin $b_{P,K}$ of closed loop with fixed-state feedback designed at nominal point $M_0 = 2.5$: a) longitudinal and b) lateral direction.

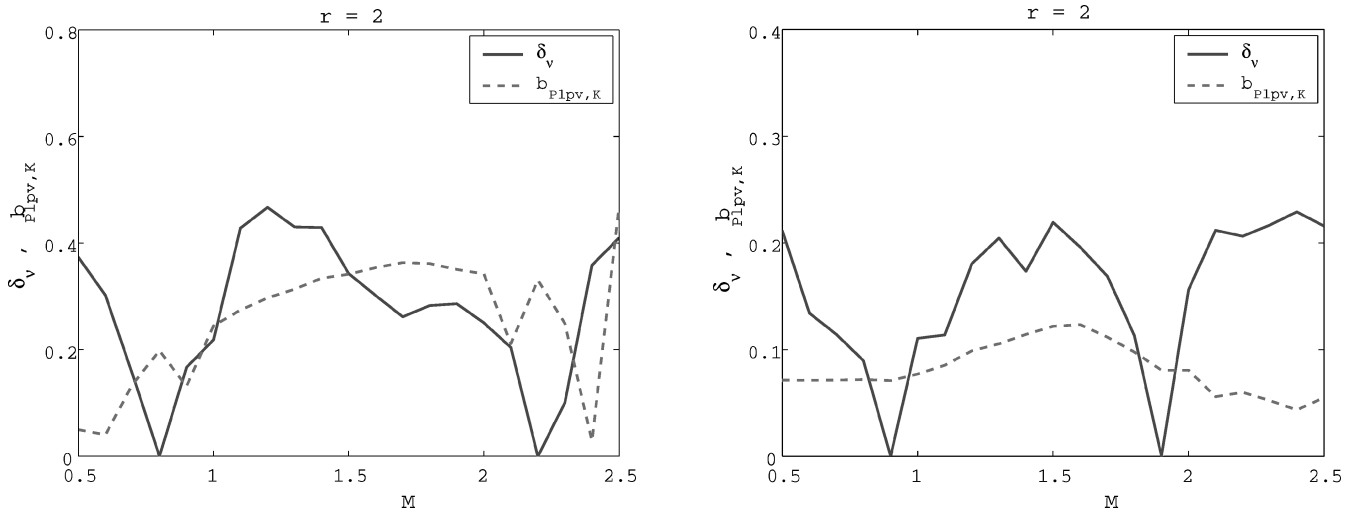


a) b)

**Fig. 6** $\nu$-gap metric $\delta_\nu[P_{\text{lpv}}(j\omega; M), P(j\omega; M)]$ between LPV and the LTI models and stability margin $b_{P_{\text{lpv}},K}$ of closed loop with gain-scheduling state feedback where $r = 2$: a) longitudinal and b) lateral direction.

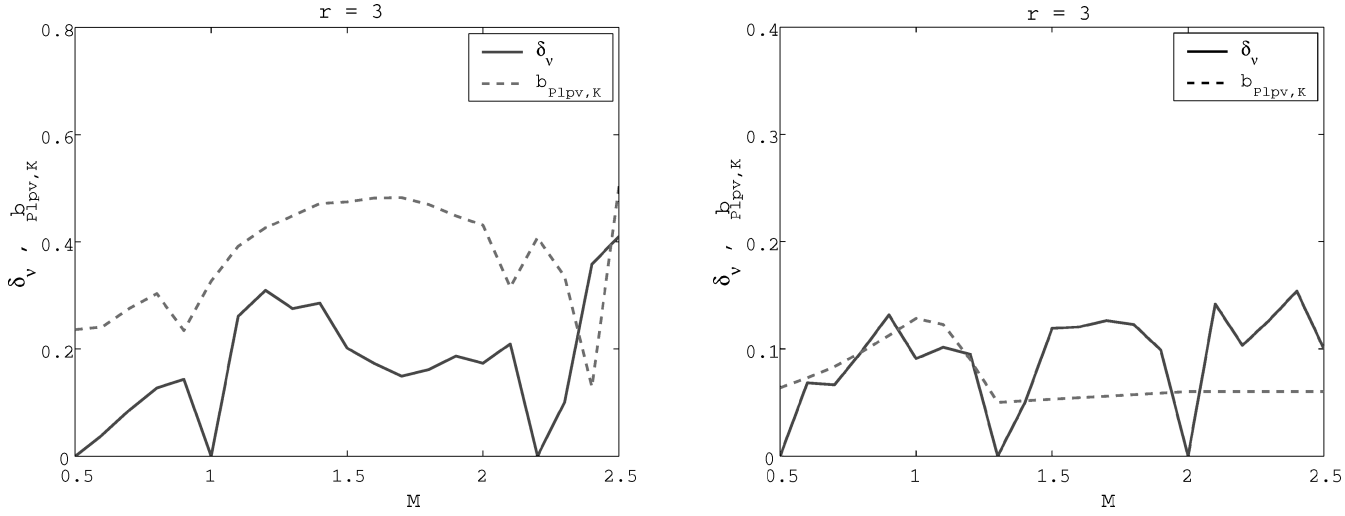


**Fig. 7** $\nu$-gap metric $\delta_\nu[P_{\text{lpv}}(j\omega; M), P(j\omega; M)]$ between LPV and the LTI models and stability margin $b_{P_{\text{lpv}},K}$ of closed loop with gain-scheduling state feedback where $r = 3$: a) longitudinal and b) lateral direction.

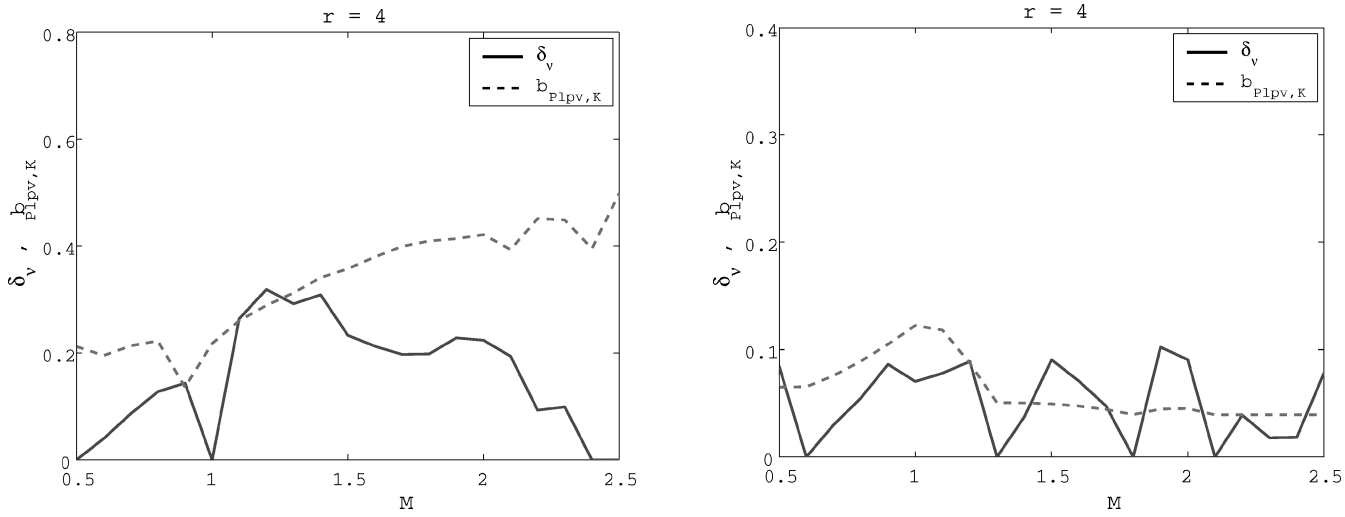


**Fig. 8** $\nu$-gap metric $\delta_\nu[P_{\text{lpv}}(j\omega; M), P(j\omega; M)]$ between LPV and the LTI models and stability margin $b_{P_{\text{lpv}},K}$ of closed loop with gain-scheduling state feedback where $r = 4$: a) longitudinal and b) lateral direction.

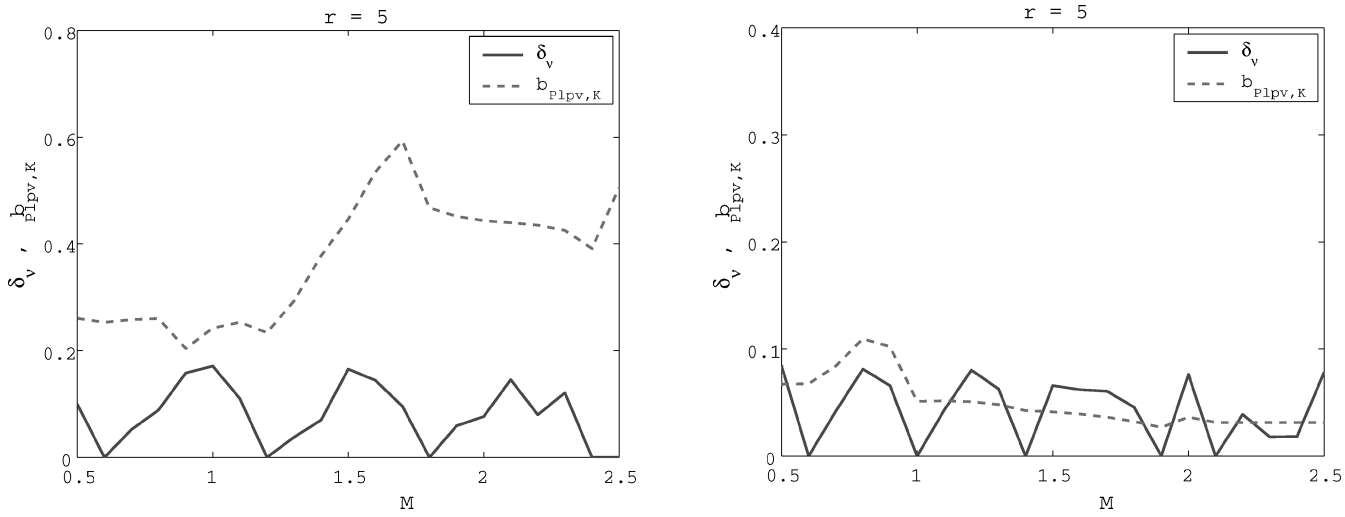


**Fig. 9** $\nu$-gap metric $\delta_\nu[P_{\text{lpv}}(j\omega; M), P(j\omega; M)]$ between LPV and the LTI models and stability margin $b_{P_{\text{lpv}},K}$ of closed loop with gain-scheduling state feedback where $r = 5$: a) longitudinal and b) lateral direction.

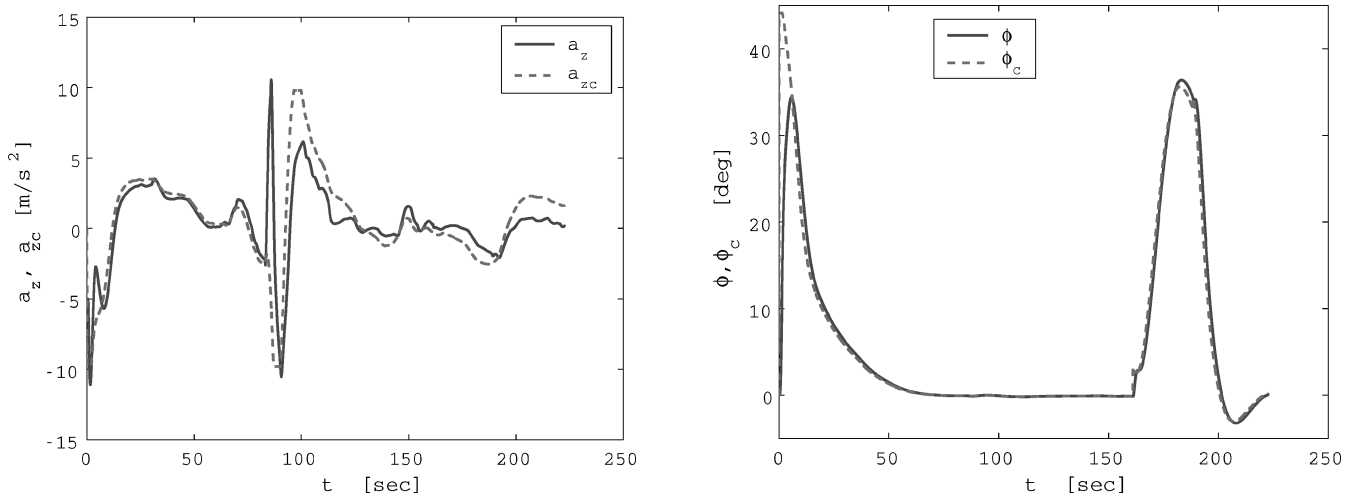


a) b)

**Fig. 10 Time responses of controlled variables using gain-scheduling state feedback where number of operating points is $r = 2$: a) vertical acceleration and b) roll angle.**

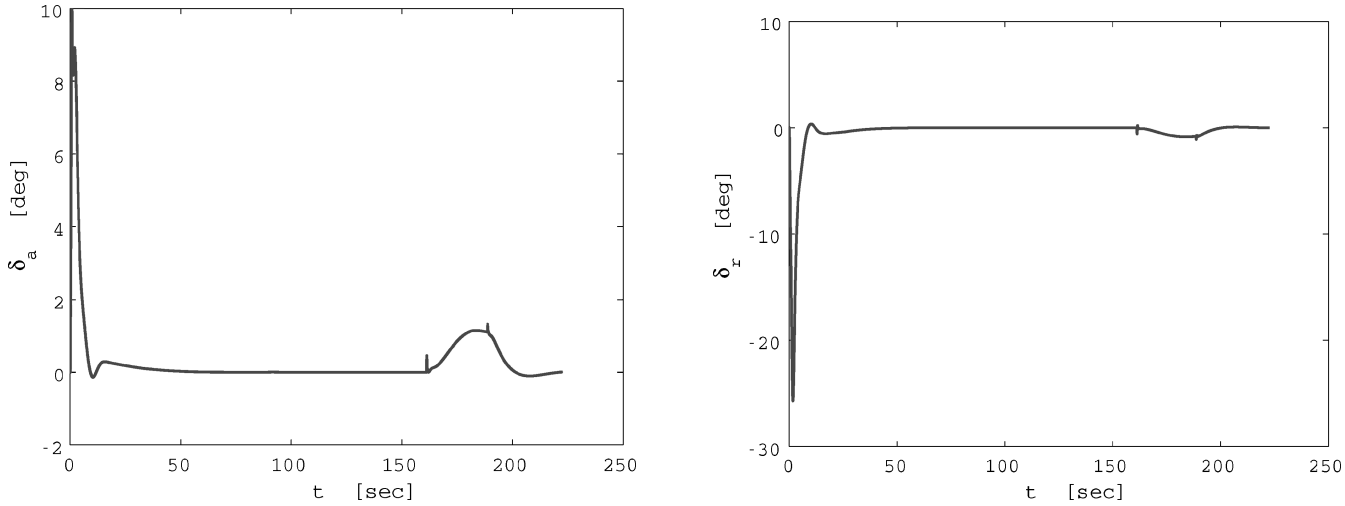


a) b)

**Fig. 11 Time responses of input variables using gain-scheduling state feedback where number of operating points is $r = 2$: a) aileron and b) rudder angle.**

The weighting matrices of the quadratic stability condition (19) were given by

$$Q = 0.01 I_4, \qquad R^{-1} = w I_2 \qquad w = 2 \tag{30}$$

As a typical simulation example, Figs. 10 and 11 respectively show time responses of the controlled and the input variables in the simulation where $r = 2$ and the operating points were selected as $M = \{0.9, 1.9\}$ to minimize $I_p$. The LTI models were obtained in the longitudinal and the lateral directions at each operating point and are shown in Appendix A. According to Eqs. (4–7), the LPV models were then constructed for both directions by linearly interpolating the LTI models. The gain-scheduling state feedback laws were obtained by solving the LMIs given in Sec. IV. The numerical values of $X_i$ and $M_i$ at $M = \{0.9, 1.9\}$ are given in Appendix B.

At the beginning of the TAEM phase, a large roll-angle command $\phi_c$ was required as shown by the dashed line. The roll angle of the HOPE-X vehicle $\phi$ almost tracked to the command $\phi_c$. The designed gain-scheduling control laws then stabilized the HOPE-X vehicle over the entire TAEM phase as shown in these figures. The simulation results where $r = 3$, 4, and 5 were almost similar to Figs. 10 and 11. Furthermore, there were no significant differences in the simulation results between min $I_p$ and min $I_a$.

For comparing the proposed gain-scheduling control with the fixed gain control, fixed-state feedback laws were designed at $M = 2.5$, 1.5, and 0.5. Figures 12 and 13, respectively, show time responses of the controlled and the input variables where the state feedback laws were designed at $M = 2.5$. The HOPE-X vehicle was stabilized until about 80 s, but destabilized after that as a result of increasing model error especially in the lateral direction. The state feedback laws designed at $M = 1.5$ and 0.5 could not stabilize the HOPE-X vehicle for the initial roll command. This destabilization was caused by increasing the $\nu$-gap metric and decreasing the stability margin of the fixed-gain control law.

To evaluate the necessity of gain scheduling for the HOPE-X, fixed-state feedback laws designed by linear-quadratic-regulator (LQR) and gain-scheduling laws were applied to both the longitudinal and the lateral directions. Table 1 summarizes the simulation results. Fix means fixed-gain state feedback law designed by LQR and corresponds to the case $r = 1$, whereas GS means the proposed gain-scheduling state feedback law and corresponds to the cases $r = 2$–5; ◯ indicates that the flight in TAEM phase was successfully completed, whereas × indicates that the flight failed (the vehicle destabilized). The fixed-gain control was not sufficient for the lateral direction control because the variation of lateral LTI models of the HOPE-X vehicle was too large to robustly stabilize the vehicle in the TAEM phase. Moreover, the preceding result also relates to the fact that the stability margin in the lateral direction (Figs. 6b–9b) was not so large that in the longitudinal direction (Figs. 6a–9a).

Summarizing the preceding, gain scheduling was needed for the lateral direction to stabilize the HOPE-X vehicle in the entire TAEM phase. The number of the operating points greater than two, $r \geq 2$, were required to stabilize the HOPE-X vehicle and track the guidance commands.

### C. Local Multi-Objective Gain Scheduling

As discussed in the preceding section, the HOPE-X vehicle was stabilized and tracked the commands by the gain-scheduling state feedback when the number of the operating points was $r \geq 2$. However, the gain-scheduling state feedback laws did not always stabilize the HOPE-X vehicle. When a large roll-angle command $\phi_c$ was applied at the beginning of the TAEM phase, the nonlinearities in the HOPE-X vehicle were not negligible. In such situation, the high-gain state feedback laws led to saturation of control surfaces and the HOPE-X vehicle was de-stabilized.

To avoid this, an input-saturation constraint (25), that is, LMIs (28), was added to the gain-scheduling state feedback laws. Figures 14 and 15 show the initial responses of the control surfaces, $\delta_a$ and $\delta_r$, at $M = 0.7$ and 2.1, respectively. The solid line is the response with the input-saturation constraint, whereas the dashed-line is the one without the constraint. As seen in these figures, the amplitude of the control surface angles was suppressed by imposing the input-saturation constraint LMIs (28). Table 2 shows the weight $w$ of Eq. (30) for obtaining successful gain-scheduling state feedback, that is, where the flight in the TAEM phase was successfully

**Table 1 Simulation results in TAEM phase**

| Longitudinal | Lateral | $r=1$ | $r=2$ | $r=3$ | $r=4$ | $r=5$ |
|---|---|---|---|---|---|---|
| Fix[a] | Fix | ×[b] | —— | —— | —— | —— |
| Fix | GS[c] | —— | ◯ | ◯ | ◯ | ◯ |
| GS[b] | Fix | —— | × | × | × | × |
| GS | GS | —— | ◯ | ◯ | ◯ | ◯ |

[a]Fix = fixed-gain state feedback law designed by LQR.
[b]× = flight failed (the vehicle was destabilized).
[c]GS = proposed gain-scheduling state feedback law.
[d]◯ = flight in TAEM phase was successfully completed.

**Table 2 Range of $w$ in which state feedback law stabilized the HOPE-X vehicle and tracked the guidance command over the entire TAEM phase**

| $r$ | Index | With $V < \rho^2$ | Without $V < \rho^2$ |
|---|---|---|---|
| 2 | $I_p$ | $3 \leq w \leq 207$ | $0.1 \leq w \leq 92$ |
| | $I_a$ | $2 \leq w \leq 729$ | $0.03 \leq w \leq 210$ |
| 3 | $I_p$ | $3 \leq w \leq 528$ | $0.02 \leq w \leq 68$ |
| | $I_a$ | $2 \leq w \leq 885$ | $0.02 \leq w \leq 130$ |
| 4 | $I_p$ | $2 \leq w \leq 587$ | $0.01 \leq w \leq 122$ |
| | $I_a$ | $5 \leq w \leq 701$ | $0.01 \leq w \leq 108$ |
| 5 | $I_p$ | $5 \leq w \leq 888$ | $0.01 \leq w \leq 92$ |
| | $I_a$ | $5 \leq w \leq 800$ | $0.1 \leq w \leq 90$ |

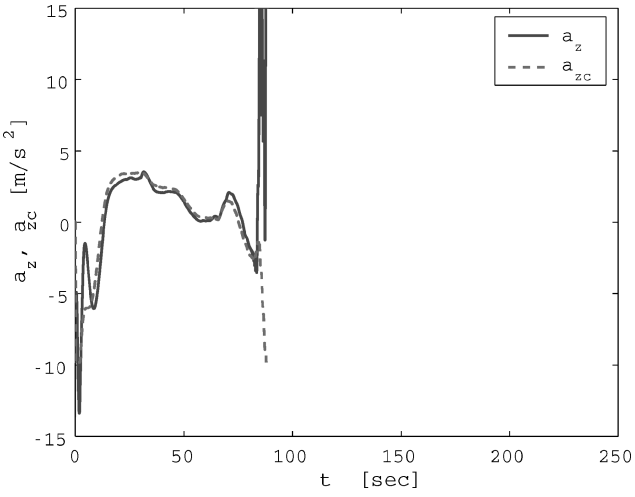


a)

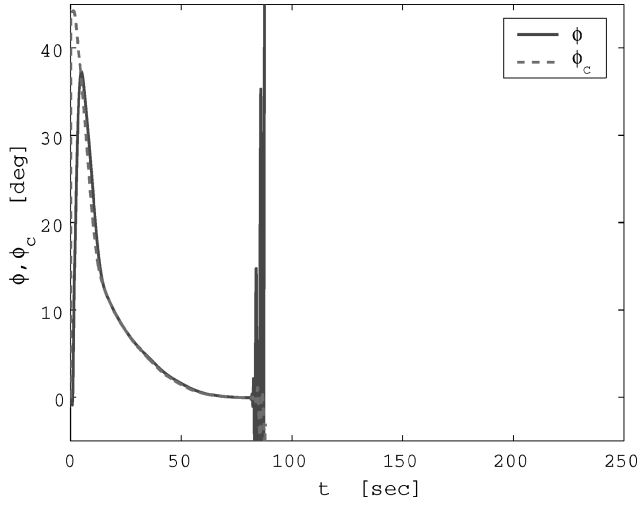


b)

**Fig. 12 Time responses of controlled variables using fixed-gain state feedback: a) vertical acceleration and b) roll angle.**

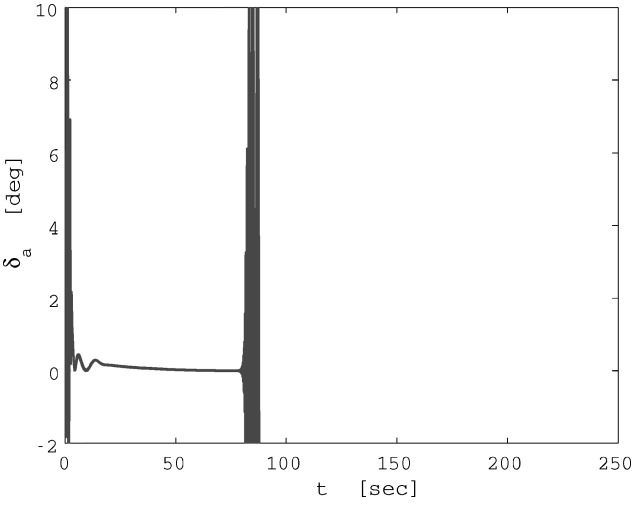


a)

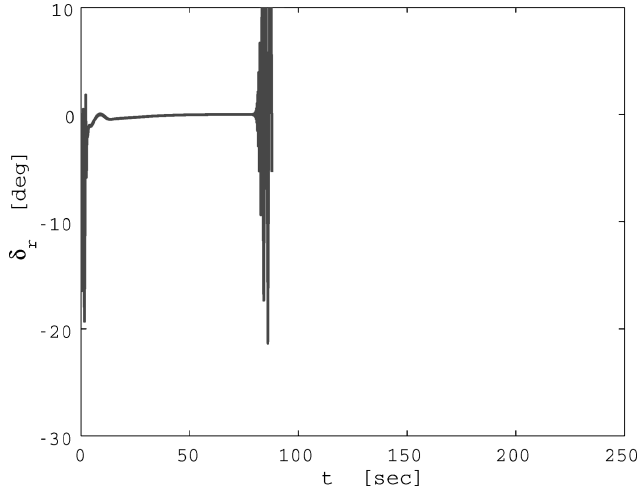


b)

**Fig. 13 Time responses of input variables using fixed-gain state feedback: a) aileron and b) rudder angle.**

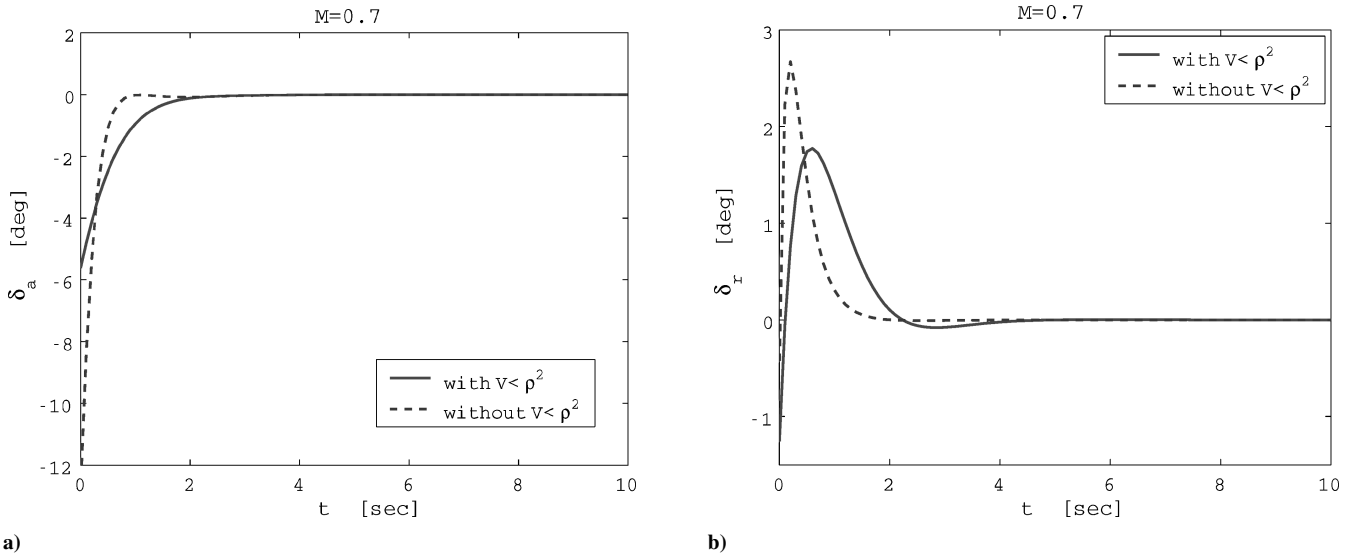


**Fig. 14 Initial responses of control surfaces at $M = 0.7$: a) aileron and b) rudder angle.**

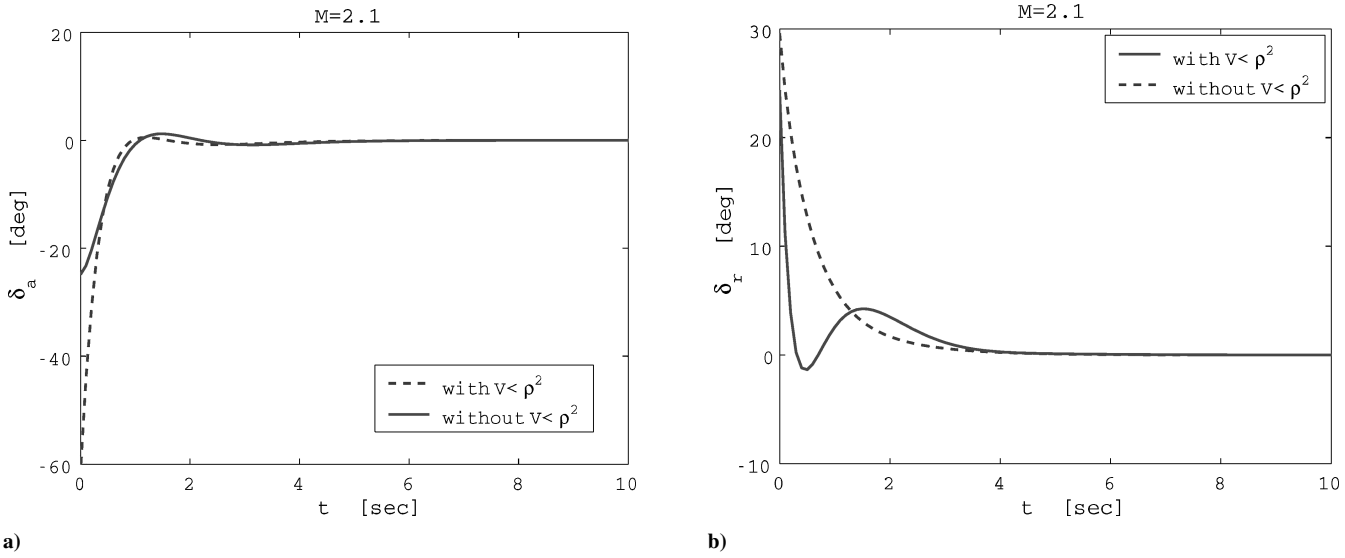


**Fig. 15 Initial responses of control surfaces at $M = 2.1$: a) aileron and b) rudder angle.**

completed. Thus, the input-saturation constraint (25) was effective in extending the range of $w$.

## VI. Conclusions

A flight control design for an unmanned space vehicle, the HOPE-X, has been presented using an interpolative gain-scheduling technique. The $\nu$-gap metric was used to evaluate the interpolative error between linear models at the operating points. Linear-parameter-varying (LPV) models for the HOPE-X vehicle were then constructed by minimizing a criterion using the $\nu$-gap metric. Two types of criteria were proposed in this paper. Multi-objective constraints were locally imposed on the operating region to improve the control performance. In the numerical simulations of the HOPE-X in the terminal-area energy-management (TAEM) phase, gain scheduling was needed for the lateral direction control because the variations of the lateral linear-time-invariant models of the HOPE-X vehicle were too large to robustly stabilize it. The number of the operating points had to be greater than two to stabilize the HOPE-X vehicle over the entire region of the TAEM phase. Furthermore, an additional constraint, the input-saturation constraint, was effective in suppressing the magnitude of the control surface angles and extending the stability region of the design parameter. For nonlinear aerospace vehicles such as the HOPE-X, dynamic inversion control is one of the more powerful control design techniques which can be used. Therefore, a future topic for research is the comparison of the proposed gain-scheduling technique to the dynamic inversion in the numerical simulation of the HOPE-X. To evaluate the robustness of the control system, the flight simulation should be performed with several kinds of uncertainties. Monte Carlo simulation[5] is one of methods to do this.

## Appendix A: Numerical Data of LTI Model

The numerical data of the LTI models at $M = \{0.9, 1.9\}$ were as follows. The LPV models were then constructed by linearly interpolating these LTI models.

1)

$$M = 0.9$$

a) Longitudinal LTI model:

$$A_1 = \begin{bmatrix} -0.6027 & 1 \\ -0.7467 & 0 \end{bmatrix}, \qquad B_1 = [-0.1353 \; -6.0839]$$

$$C_1 = [-2.89330], \qquad D_1 = -0.6381$$

b) Lateral LTI model:

$$A_1 = \begin{bmatrix} -0.1386 & 0.0777 & -0.9970 & 0 \\ -21.5133 & 0 & 0 & 0 \\ -0.4871 & 0 & 0 & 0 \\ -0.0001 & 1 & -0.4632 & 0 \end{bmatrix}$$

$$B_1 = \begin{bmatrix} 0.0238 & 0.0420 \\ 21.5416 & 6.3686 \\ -1.0405 & -2.0356 \\ 0 & 0 \end{bmatrix}$$

$$C_1 = \begin{bmatrix} 0 & 0 & 0 & 1 \\ -0.7490 & 0 & 0 & 0 \end{bmatrix}, \qquad D_1 = \begin{bmatrix} 0 & 0 \\ 0.1103 & 0.1946 \end{bmatrix}$$

2)

$$M = 1.9$$

a) Longitudinal LTI model:

$$A_2 = \begin{bmatrix} -0.1347 & 1 \\ -0.3048 & 0 \end{bmatrix}, \qquad B_2 = \begin{bmatrix} -0.0157 \\ -1.7791 \end{bmatrix}$$

$$C_2 = [-1.4291 \quad 0], \qquad D_2 = -0.1551$$

b) Lateral LTI model:

$$A_2 = \begin{bmatrix} -0.0380 & 0.0875 & -0.9962 & 0 \\ -2.5777 & 0 & 0 & 0 \\ -0.9481 & 0 & 0 & 0 \\ -0.0001 & 1 & -0.0642 & 0 \end{bmatrix}$$

$$B_2 = \begin{bmatrix} 0.0013 & 0.0043 \\ 4.2452 & 1.0789 \\ -0.1617 & -0.5060 \\ 0 & 0 \end{bmatrix}$$

$$C_2 = \begin{bmatrix} 0 & 0 & 0 & 1 \\ -0.4712 & 0 & 0 & 0 \end{bmatrix}, \qquad D_2 = \begin{bmatrix} 0 & 0 \\ 0.0130 & 0.0426 \end{bmatrix}$$

## Appendix B: Gain-Scheduling State Feedback

Using the matrices given in Appendix A, the gain-scheduling state feedback laws were obtained by solving the LMIs given in Sec. IV. The numerical values of matrices $X_i$ and $M_i$ at $M = \{0.9, 1.9\}$ were as follows:

1)

$$M = 0.9$$

a) Longitudinal direction:

$$X_1 = \begin{bmatrix} 31.3892 & -12.1211 \\ -12.1211 & 33.8891 \end{bmatrix}, \qquad M_1 = [-1.1102 \quad -9.8131]$$

b) Lateral direction:

$$X_1 = \begin{bmatrix} 26.5760 & 8.9343 & 33.3948 & 3.0601 \\ 8.9343 & 150.6468 & 6.6549 & -45.3181 \\ 33.3948 & 6.6549 & 49.4580 & 3.6242 \\ 3.0601 & -45.3181 & 3.6242 & 55.6260 \end{bmatrix}$$

$$M_1 = \begin{bmatrix} -25.5476 & -0.0991 & -25.6215 & -0.3973 \\ 1.1970 & 6.5249 & -23.8548 & 2.5219 \end{bmatrix}$$

2)

$$M = 1.9$$

a) Longitudinal direction:

$$X_2 = \begin{bmatrix} 38.1981 & -16.3596 \\ -16.3596 & 35.0281 \end{bmatrix}, \qquad M_2 = [-4.8354 \quad -18.5972]$$

b) Lateral direction:

$$X_2 = \begin{bmatrix} 25.6727 & -3.3825 & 27.9274 & 4.1756 \\ -3.3825 & 100.9669 & -3.3443 & -41.3308 \\ 27.9274 & -3.3443 & 32.4675 & 2.4296 \\ 4.1756 & -41.3308 & 2.4296 & 66.3161 \end{bmatrix}$$

$$M_2 = \begin{bmatrix} -20.9356 & 25.2574 & -19.7562 & 2.6915 \\ 4.0080 & -0.2351 & -11.6474 & 1.7222 \end{bmatrix}$$

## References


[1]Davis, N. W., "NASDA Pins Its Hopes on HOPE," *Aerospace America*, Aug. 1991, pp. 32–35.

[2]Shibato, Y., "Overview of Reusable Space Transportation System Development Plan," *Proceedings of the ALFLEX Symposium*, Tokyo, 1998, pp. 1–6.

[3]Tsujimoto, T., et al., "Development of the H-II Orbiting Plane-Experimental (HOPE-X)," *Proceedings of the 21st ISTS*, Tokyo, 1998, pp. 1189–1194.

[4]Yanagihara, M., Miyazawa, Y., and Taniguchi, H., "Simulation Analysis of the HOPE-X Demonstrator," AIAA Paper 99-4875, Aug. 1999.

[5]Miyazawa, Y., Motoda, T., Izumi, T., and Hata, T., "Longitudinal Landing Control Law for an Autonomous Reentry Vehicle," *Journal of Guidance, Control, and Dynamics*, Vol. 22, No. 6, 1999, pp. 791–800.

[6]Fujimori, A., Tsunetomo, H., and Wu, Z.-Y., "Gain-Scheduled Control Using Fuzzy Logic and Its Application to Flight Control," *Journal of Guidance, Control, and Dynamics*, Vol. 22, No. 1, 1999, pp. 175–178.

[7]Fujimori, A., Kurozumi, M., Nikiforuk, P. N., and Gupta, M. M., "Flight Control Design of an Automatic Landing Flight Experiment Vehicle," *Journal of Guidance, Control, and Dynamics*, Vol. 23, No. 2, 2000, pp. 373–376.

[8]Fujimori, A., Nikiforuk, P. N., and Gupta, M. M., "A Flight Control Design of a Reentry Vehicle Using Double Loop Control System with Fuzzy Gain-Scheduling," *Journal of Aerospace Engineering*, Vol. 215, No. G1, 2001, pp. 1–12.

[9]Fujimori, A., Nagasaka, M., and Terui, F., "Flight Control Designs of an Unmanned Space Vehicle Using Linear Interpolation Gain Scheduling," *Transactions of JSASS*, Vol. 50, No. 582, 2002, pp. 278–285 (in Japanese).

[10]Morth, R., "An Explicit at Automatic Terminal Energy Management Guidance Technique for Space Shuttle," AIAA Paper 72-833, Jan. 1972.

[11]Boyd, S., Ghaoui, L. E., Feron, E., and Balakrishnan, V., *Linear Matrix Inequalities in System and Control Theory*, Vol. 15, Society of Industrial and Applied Mathematics, Philadelphia, 1994.

[12]Vinnicombe, G., *Uncertainty and Feedback ($H_\infty$ Loop-Shaping and the $\nu$-Gap Metric)*, Imperial College Press, London, 2001.

[13]McFarlane, D. C., and Glover, K., *Robust Controller Design Using Normalized Coprime Factor Plant Descriptions*, Springer-Verlag, London, 1990.

[14]Gahinet, P., Apkarian, P., and Chilali, M., "Affine Parameter-Dependent Lyapunov Functions for Real Parametric Uncertainty," Proceedings of CDC, 1994, pp. 2026–2031.